Liu Zhifei (Orcid ID: 0000-0002-5202-6283)

Reconstructing chemical weathering intensity in the Mekong River basin since the Last Glacial Maximum

Thanakorn Jiwarungrueangkul[1], Zhifei Liu[1]*, Karl Stattegger[2,3], Pham Nhu Sang[1]

[1]State Key Laboratory of Marine Geology, Tongji University, Shanghai 200092, China

[2]Institute of Geosciences, University of Kiel, 24118 Kiel, Germany

[3]Institute of Geology, Adam Mickiewicz University, 61-712 Poznań, Poland

*Corresponding author. E-mail address: lzhifei@tongji.edu.cn (Z. Liu)

Key Points:

1. The Mekong River is the major terrigenous sediment contributor to the southwestern South China Sea.
2. Chemical weathering intensity in the Mekong River basin has been moderate since the Last Glacial Maximum.
3. Intensity of chemical weathering in the Mekong River basin is controlled by the East Asian summer monsoon evolution.

This article has been accepted for publication and undergone full peer review but has not been through the copyediting, typesetting, pagination and proofreading process which may lead to differences between this version and the Version of Record. Please cite this article as doi: 10.1029/2019PA003608

Abstract

High-resolution clay mineralogy and major element geochemistry of Core SO18383-3 collected off the Mekong River mouth in the southern South China Sea have been investigated, aiming to reconstruct sediment provenance and chemical weathering intensity since the last glaciation. The chronology is based on foraminiferal AMS ^{14}C dates. Clay mineral analysis suggests that the Mekong River is a major sedimentary source for the studied area. The values of chemical index of alteration (CIA) indicate moderate chemical weathering in the Mekong River basin. Smectite/(illite + chlorite) and smectite/kaolinite ratios coupled with TiO_2/K_2O ratio reveal the temporal variation in chemical weathering intensity in the Mekong River basin. The lower ratios around the Last Glacial Maximum (LGM) (29.9–14.7 cal ka BP), the Heinrich Event 1 (~14.8 cal ka BP), the Younger Dryas interval (12.4–11.3 cal ka BP), and mid to late Holocene (7.6–1.1 cal ka BP) indicate weak chemical weathering intensity. In contrast, the higher ratios occurring during the Bølling-Allerød period (14.7–12.6 cal ka BP) and the period of main deglaciation (14.7–7.6 cal ka BP) indicate stronger chemical weathering in the Mekong River basin. The good correlations between these proxies and the available proxy records of the East Asian summer monsoon intensity suggest that the intensity of chemical weathering in the Mekong River basin over the last 30 ka is significantly controlled by the summer monsoon. This study greatly increases our understanding of the principal forcing factor on continental weathering in the Mekong River basin since the LGM.

Key words: chemical weathering intensity, clay mineralogy, geochemistry, Mekong River, South China Sea

1. Introduction

The chemical weathering on land is the primary process responsible for topographic evolution and exerts a major control on the terrigenous sediment transport from the land to the sea (Riebe et al., 2004; Limmer et al., 2012b; Zhao, D. et al., 2018). It also plays a critical role in the global climate change by regulating atmospheric carbon dioxide concentrations on geological timescales (Ludwig et al., 1999; Riebe et al., 2004; Wan et al., 2017). In general, the continental weathering processes are regulated and complicated by several factors including climate, tectonics, and lithology at various scales (Meybeck, 1987; Oliva et al., 2003; Liu et al., 2012). However, climatic condition has typically been regarded as the primary determinant of continental weathering (Liu et al., 2005; Wei et al., 2006; Clift et al., 2008). A stronger chemical weathering rate correlates to more humid and warm climates. Meanwhile, weaker chemical weathering relates to drier climates (Liu et al., 2005; Colin et al., 2006). However, some studies argue that strong physical erosion may be also related to a warm climate, when monsoon rainfall increases, owing to faster run-off in the absence of drainage capture (Dadson et al., 2003; Clift et al., 2014; Zhao et al., 2017). Consequently, the interaction of chemical weathering with climatic conditions remains elusive and needs more investigation. Southeast Asia has very high input of weathered sediments that can provide invaluable information on the evolution of continental weathering (Milliman et al., 1999; Liu et al., 2005, 2012; Clift et al., 2004; Huang et al., 2016). Comparing the amount of fluvial discharge from rivers in this region, the Mekong River is regarded as the primary fluvial system to supply terrigenous sediments to the South China Sea (SCS) (Milliman et al., 1999; Liu & Stattegger, 2014; Fig. 1). The Mekong River is 4,350 km long, originates on the Tibetan Plateau, drains large parts of southwestern China, Myanmar, Thailand, Laos, Cambodia, and Vietnam, and finally enters the southern SCS through the Mekong Delta (Fig. 1). The Mekong River has a drainage basin of 810,000 km^2, with an annual sediment discharge of 160 million tons (Milliman and Syvitski, 1992), making it the longest and largest river by volume in Southeast Asia, and the 12th longest and 8th largest by volume in the world. In the Mekong River basin,

climatic setting is strongly dominated by the East Asian monsoon that plays an important role for the river hydrology and river derived sediments (Debenay and Luan, 2006; Xue et al., 2012; Unverricht et al., 2013). Such a large basin in the East Asian monsoon region and a huge input of terrigenous sediments from the land, the Mekong River basin is an ideal area to study the weathering history of silicate weathering processes that can increase our understanding of the principal forcing factor on continental weathering interacting with variations of the East Asian monsoon in South China and Southeast Asia regions.

As direct weathering products of continental rocks, clay minerals and elements of terrigenous sediments can provide the most powerful tool for reconstructing the chemical weathering history (Liu et al., 2005; Miriyala et al., 2017; Wan et al., 2017; Zhao et al., 2018). In the Mekong River basin, a study of Liu et al. (2004, 2005) employed clay minerals and elements as chemical weathering proxy over the past 190 ka, showing strengthened chemical weathering corresponding to increased sediment discharge and weakened physical erosion during interglacial periods; in contrast, weakened chemical weathering is associated with reduced sediment discharge and intensified physical erosion during glacial periods. Meanwhile, Colin et al. (2010) implied that higher chemical weathering of detrital material originates mainly from the lower reach of the Mekong River basin over the past 25 ka. However, these previous studies do not reveal a chemical weathering status within the Mekong River basin such as chemical index of alteration (CIA) that is more sensitive measure of the degree of chemical weathering and the most accepted weathering indicator (Nesbitt and Young, 1982). Moreover, how chemical weathering in the Mekong River basin responds to the rapid changes of the East Asian monsoon, i.e., Heinrich Events (H1 and H2), Bølling–Allerød (B/A), and Younger Dryas (YD) (Wang et al., 2001; Dykoski et al., 2005), remains poorly understood because of lack of high resolution study in this area. Therefore, a comprehensive study of high resolution terrigenous-based proxies that can indicate a quantitative degree of chemical weathering in the Mekong River basin needs to be examined. This would help to enhance understanding of an integrated weathering history and continental weathering

relating to variations of the East Asian monsoon climate. In this study, we adopt proxies that combine measurements of clay minerals and major elements to assess the history of chemical weathering intensity and weathering status. High-resolution clay mineralogy and major element geochemistry are investigated in the gravity Core SO18383-3 recovered off the Mekong River mouth in the southern SCS. The objectives of this study are to (1) identify the main sediment provenance in this area, (2) reveal the quantitative degrees of chemical weathering in the Mekong River basin, and (3) reconstruct the history of chemical weathering intensity in response to changes in the East Asian monsoon since the Last Glacial Maximum (LGM).

2. Material and methods

2.1 Material

The gravity Core SO18383-3 (7º38.54'N, 109º29.15'E; 710.6 m water depth; 9.44 m long) was retrieved on the continental slope off the Mekong River mouth in the southern SCS during the cruise SO-140 on RV *SONNE* (Fig. 1). The upper 1.0 m in the studied core is composed of olive gray homogeneous silt and clay; the lower section from 1.0 m depth to the base of the core is dominated by dark greenish gray homogeneous silt and clay (Fig. 2). This sediment core was sampled at a resolution of 4 cm, obtaining 237 samples in total. All samples were analyzed for carbonate content and clay minerals. Among them, a total of 166 samples, taken every 4 cm interval down to 4 m and every 8 cm interval from 4 m to the base, were analyzed for major elements. Six foraminiferal samples from different depths were used for measuring accelerator mass spectrometry (AMS) ^{14}C dating for reconstructing the age model.

2.2 Analytical methods

All clay mineral and geochemical analyses except AMS ^{14}C dating were processed at the State Key Laboratory of Marine Geology, Tongji University. Clay minerals were identified by X-ray diffraction (XRD) using a PANalytical X'Pert PRO diffractometer on oriented mounts of non-calcareous, clay-sized particles (Holtzapffel, 1985). Pretreatment of oriented mounts and

measurements were based on the method described by Liu et al. (2004). After the removal of carbonate and organic matter, the clay minerals (<2 μm) were separated using the principle of Stokes' settling velocity. The extracted clay minerals were smeared on the surface of the glass slides, and they were then dried at room temperature. Three XRD runs were performed under air-dried, ethylene-glycol solvation for 24 hours, and heating at 490°C for 2 hours. Identification and interpretation of the clay minerals were made mainly according to the (001) basal reflections on the three XRD diagrams. Semi-quantitative estimates of peak areas of the basal reflections for smectite (including mixed-layers) (15–17 Å), illite (10 Å), and kaolinite/chlorite (7 Å) were carried out on the glycolated curve by using the MacDiff software. Relative proportions of kaolinite and chlorite were separated by relative proportions according to the 3.57/3.54 Å peak areas. Moreover, some mineralogical characters of illite were determined on the glycolated curve. The illite crystallinity was expressed as the full width at half maximum (FWHM) of the illite 10 Å peak. Meanwhile, the illite chemical index was estimated from the 5/10 Å illite peak areas (Esquevin, 1969).

Analysis of major elements was performed on bulk sediments by X-ray fluorescence (XRF), using a PANalytical Axios MAX Spectrometer. The dried sediments were ground to powder with an agate pestle and mortar. About 4 g of the powder was mixed with H_3BO_3 in a set of cylinder mold, and then compressed with 200 kN. Overall analytical precision and accuracy were monitored by measurements of the national geostandards GSR-6 and GSD-15 provided by National Research Center for Geo-analysis of marine sediments. The results were in the range of the verified values.

AMS ^{14}C dating and carbonate stratigraphy were analyzed in order to establish a reliable age model. For four samples on the upper part of the core with relatively high carbonate contents, more than 8 mg of well-preserved planktonic *Globigerinoides ruber* shells (no size limits) were picked from each sample for AMS ^{14}C dating. However, the glacial sediments in the lower part of the core contain very low carbonate contents (<5%), resulting in insufficient planktonic foraminifera (*G. ruber*, even together with other planktonic species). We then picked more

than 8 mg of mixed species of planktonic and benthic foraminifera (including *G. ruber*, *Uvigerina sp., Cibicidoides sp.,* and *Bulimina sp.*) from each sample for two samples in the bottom part for AMS ^{14}C dating. Although the benthic foraminifera should give slightly older ages than those from the planktonic foraminifera (Wan and Jian, 2014), the mixture of planktonic and benthic foraminifera from the similar glacial sediments in the southern SCS can provide an acceptable AMS ^{14}C dating (Jiwarungrueangkul et al., 2019). The AMS ^{14}C dating was done at Beta Analytic Laboratory, USA. The carbonate content was determined by a reaction with HCl in a pressure calcimeter that had been calibrated. Before the analysis, the bulk samples were ground to powder with an agate pestle and mortar. One in every 10 samples was determined in replication for quality control. The values of relative standard deviation of the replicate samples were less than 2%.

3. Results

3.1 Age model

The AMS ^{14}C datings of Core SO18383-3 are reported in Table 1. The age model of Core SO18383-3 was established by using AMS ^{14}C data. The six AMS ^{14}C data were calibrated to the calendar year before present (cal yr BP) using the Bayesian age-depth model (Fig. 2). The Bayesian age-depth model implemented in R version 3.6.0 with a Bacon age-modelling (Blaauw and Christen, 2011) and the updated age-calibration curve of Marine13 (0–50,000 cal yr; Reimer et al., 2013). The general pattern of carbonate content of the studied core are within the range of 4% to 38%, with a relatively high percentage during the Holocene and high percentage in glacial time (Fig. 2), in agreement with previous studies in the southern SCS (e.g., Steinke et al., 2003; Zhao et al., 2006; Li et al., 2010; Jiwarungrueangkul et al. 2019), supporting our age model. The investigated interval of the studied core has a basal age of 29.9 cal ka BP. The linear sedimentation rate varies in the range of 15–53 cm/ka, with an average of 32 cm/ka (Fig. 2). There is clear evidence that the sedimentation rate of Core 18383-3 in the Late Pleistocene was higher than that of the Holocene with higher values during early stages of deglaciation and lower values during mid and late Holocene.

3.2 Clay minerals

The clay mineral assemblage of Core SO18383-3 consists mainly of smectite (25–58%) and illite (19–38%), with a minor abundance of chlorite (12–21%) and kaolinite (11–19%) (Fig. 3). Generally, illite and chlorite contents show a similar pattern throughout the record. The distribution patterns of illite and chlorite show relatively higher contents between 29.9 and 17.1 cal ka BP. Meanwhile, they display gradually decreasing contents after the Heinrich Event 1 (17.1 cal ka BP) and then are stable during 7.6–1.1 cal ka BP (Fig. 3). The pattern of kaolinite content is generally similar to illite and chlorite contents. It presents a gradually increasing trend during 29.9–13.2 cal ka BP and a decreasing trend between 13.2–7.6 cal ka BP, followed by a slightly increasing trend over the last 7.6 ka. Smectite exhibits no correspondence with those three clay minerals. It shows lower contents during the interval of 29.9–17.1 cal ka BP but increases gradually since the Bølling-Allerød period (around 14.7 cal ka BP), and conversely decreases gradually over the last 7.6 ka. The illite crystallinity varies between 0.15 and 0.21 $\Delta^{\circ}2\theta$ with an average value of 0.18 $\Delta^{\circ}2\theta$, showing a decreasing trend from around 14.8 cal ka BP. Meanwhile, the illite chemical chemistry index shows a narrow range of 0.36 to 0.49 (average 0.41) without a systematic trend (Fig. 3).

3.3 Major elements

Major element distribution in Core SO18383-3 sediments consists mainly of SiO_2 (45.5–57.7%), Al_2O_3 (14.1–17.9%), Fe_2O_3 (5.1–6.9%), CaO (3.0–11.9%), MgO (2.2–2.6%), Na_2O (1.3–1.8%), and K_2O (2.6–3.3%) with a low content of TiO_2 (0.6–0.8%) (Fig. 4). Temporal patterns of Al_2O_3, Fe_2O_3, SiO_2, K_2O, and TiO_2 are basically similar in their distribution. The sediments between 29.9 and 14.7 cal ka BP are characterized by high contents of these elements. Meanwhile, these elements show a gradual decrease since the Bølling-Allerød period (14.7 cal ka BP) and reach stable low contents during 7.6–1.1 cal ka BP or a slight increase during the late Holocene (Al_2O_3 and K_2O) (Fig. 4). In contrast, temporal variations of CaO, MgO, and Na_2O show generally an inverse correlation to Al_2O_3. Elements CaO, MgO, and Na_2O show lower contents from 29.9 to 14.7 cal ka BP followed by a gradual increase

during 14.7–7.6 cal ka BP. The contents of these elements remain again stable over the last 7.6 ka or decrease slightly during the late Holocene (CaO) (Fig. 4).

4. Discussion

4.1 Provenance analysis

The potential source and transport process of terrigenous sediments deposited in a marginal sea are required in reconstructing paleoenvironment (Liu et al., 2005; Wan et al., 2010; Huang et al., 2016). Clay minerals that are formed under influences of climatic condition, tectonic activity, and lithology in the source area are a useful tool to constrain the provenance of fine-grained terrigenous sediments in marine sediments (Biscaye, 1965), and several previous studies have successfully achieved using clay mineralogy for studying sediment provenances in the SCS (e.g., Liu et al., 2004; Steinke et al., 2008; Chen et al., 2017; Zhao S. et al., 2018; Jiwarungrueangkul et al., 2019). Because of low eolian fluxes in the southern SCS (Wehausen et al. 2003; Liu et al., 2004), the terrigenous sediments in this region are mainly delivered by the surrounding rivers, such as the Mekong River and rivers from Borneo, Sumatra, the Malay Peninsula, and Thailand (Liu et al., 2007, 2016; Steinke et al., 2008; Huang et al., 2016; Fig. 1). In order to observe and interpret sediment provenance, the clay mineral assemblages of Core SO18383-3 and river samples of these potential sources are plotted in a ternary diagram (Fig. 5). Here, the clay mineral assemblage of Core SO18383-3 has no clear overlap with these potential sources. This could tend to the interpretation of multiple potential provenances as following previous studies (e.g., Steinke et al., 2008; Wang et al., 2015; Chen et al., 2017). However, we see strong evidence that the terrigenous sediments of the studied core could have been mainly transported from the Mekong River. Illite and chlorite have a similar distribution along the entire record (Fig. 3), suggesting that these two clays have similar sources. Therefore, illite provenance analysis is also relevant to chlorite provenance. In order to trace a significant source of illite for this site, illite chemistry index together with illite crystallinity that have been widely used to indicate the source of illite in the SCS (e.g., Liu et

al., 2007; Steinke et al., 2008; Huang et al., 2016) are plotted (Fig. 6). As illustrated in Figure 6, most of our samples are adjacent to the Mekong River samples and very different from other potential sources, indicating that illite could have been mainly contributed by the Mekong River. This also implies that the Mekong River is the main contributor of chlorite for this area. In the Mekong River basin, the highland reach that is underlain by abundant metamorphic and granitic rocks is the main source of illite and chlorite within the basin (Liu et al., 2004; 2005). Although both smectite and kaolinite should have been transported from the western sources, such as Sumatra, Malay Peninsula, and Thailand (Fig. 5), the close position of the studied core to the Mekong River mouth and inconsistency of both minerals could exclude significant contributions of smectite and kaolinite from the western sources for the following reasons (Fig. 1). Due to the fact that the western sources have high contents of kaolinite (Liu et al., 2012), enhanced summer monsoon (southwesterly) currents especially during the Holocene should transport kaolinite from the western sources to this area. However, at the studied core, kaolinite content is lower in Holocene than in Late Pleistocene sediments (Fig. 3). This inconsistency suggests that the kaolinite contribution from the western sources is less important in this area. Similarly, if smectite would be provided from western sources where there is also high content of kaolinite, an increase in smectite content should be also associated with an increase in kaolinite content. Nonetheless, they are not in correlation with each other (Fig. 3), which means that smectite originated from western sources (high smectite and kaolinite end-members) can be also excluded for this area. The trend of an increasing content of smectite from the last glacial period to the Holocene period could be linked to an enhanced input of sediments from Thailand (Fig. 5), but those are generally trapped within the Gulf of Thailand and the exchange of clay minerals between the Gulf of Thailand and the southern SCS has been very limited, due to the strong clockwise surface circulation in the entrance region during the Holocene (Liu et al., 2016; Fig. 1). Therefore, we suppose that a slightly higher content of smectite during the Holocene period could be due to the strengthened

monsoon rainfall during the Holocene (Wang et al., 2001; Dykoski et al., 2005), resulting in a higher input of smectite from the Mekong River basin (Liu et al., 2004; Colin et al., 2010).

Accordingly, we strongly suggest that both smectite and kaolinite in our core are contributed by the Mekong River, rather than by western sources. The differential settling effect of smectite in more saline and distal waters, which was reported in the SCS basin-wide clay mineral distribution (Liu et al., 2016), can explain that 4–15% smectite in the Mekong River sediments is potentially an important source for 25–58% smectite in the studied area. In Figure 5, the core samples are distributed along the extension of increased smectite end-member from the Mekong River samples. In the Mekong River basin, bisialitic soils that developed well in the middle to lower reaches of the basin could be main sources of smectite that is mainly produced by chemical weathering process (Liu et al., 2004, 2005; Colin et al., 2010). Meanwhile, ferrallitic soils located in the middle reach of the basin are major potential sources of kaolinite to the southern SCS (Liu et al., 2004, 2005). In general, kaolinite is frequently found in soils of intertropical land masses characterized by a warm, humid climate, and therefore displays a strong climatic dependence controlled by the intensity of continental hydrolysis (Chamley, 1989). In addition, kaolinite is common on steep slopes within the drainage basin. However, in Core SO18383-3, temporal variation of kaolinite contents indicates a pattern similar to those of illite and chlorite (Fig. 3). This is suggested that kaolinite in the Mekong River basin correlates to physical erosion instead of reflecting contemporary climates (e.g., Liu et al., 2005). The general consistency between higher kaolinite contents and higher linear sedimentation rates during the period around LGM could support this hypothesis (Figs. 2 and 3).

Our findings are also supported by previous studies located nearby, suggesting that a primary sediment source is the Mekong River, namely Cores MD97-2150 and MD01-2932 (Liu et al., 2004) and CG86 (Fu et al., 2011; Fig.1). Furthermore, the clay mineral assemblage of Core SO18383-3 is mostly in agreement with Core MD01-2932 (Liu et al., 2004; Colin et al., 2010; Fig. 5). Based on Liu et al. (2005), the $^{87}Sr/^{86}Sr$ and $\varepsilon_{Nd}(0)$ values of Core MD01-2393

sediments are similar to Mekong River samples, implying that the Mekong River is the major source of sediments to the margin close to the Mekong River mouth. Also, it is linearly distributed between end-members of illite + chlorite and smectite and compares closely to data from the Mekong River (Fig. 5). These evidences can support the suggestion that terrigenous sediments in this area mainly come from the Mekong River, which is the most important sediment contributor into the southern SCS, without change of dominating provenance throughout the entire record of the studied core.

4.2 Late Pleistocene and Holocene chemical weathering in the Mekong River basin

4.2.1 Intensity of chemical weathering

The chemical weathering intensity of the sediments can be revealed by a quantitative degree of chemical alteration of silicate, such as the calculated value of the CIA (Nesbitt and Young, 1982). The CIA is basically based on the relative mobility of Na, K, and Ca in aqueous fluids, compared to immobile Al that tends to be concentrated in the residues of weathered rocks. The CIA is calculated as: $CIA = [Al_2O_3 / (Al_2O_3 + CaO^* + Na_2O + K_2O)] \times 100$ (Nesbitt and Young, 1982). The CaO* represents the calcium content from the silicate fraction of the terrigenous sediments, which had been corrected for phosphate and carbonate contents in this study (Liu et al., 2007; Hu et al., 2012). Additionally, we also corrected Na_2O, K_2O, and CaO for salt. The content of excess Cl (Cl_{ex}) is used for representative of salt correction, which is defined as: $Cl_{ex} = Cl_{tot} – (0.008 \times Al_{tot})$. The Cl_{tot} and Al_{tot} are the total Cl and Al contents in the bulk sediments, while 0.008 is the Cl/Al ratio of the upper continental crust (UCC) (Taylor and Mclennan, 1985). Based on the Cl_{ex} content, the Na_2O, K_2O, and CaO contents were done by the normative method for salt correction, based on seawater composition at salinity of 35 ppt (Libes, 2009).

The CIA values recorded in Core SO18383-3 vary in the range of 71–77. As previously discussed, the terrigenous sediments in this area are mainly derived from the Mekong River; thus, the CIA values reflect significantly the chemical weathering intensity in the Mekong River basin. The CIA values of Core SO18383-3 demonstrate the moderate degree of chemical

weathering in this basin over the last 29.9 ka. The CIA values based on the bulk riverine sediments of the Mekong River are in the range of 72–83 (Liu et al., 2007), suggesting moderate to strong chemical weathering in the Mekong River basin during present time.

To better understand the alteration of geochemical behaviors during weathering process, the percentage changes of Na_2O and K_2O relative to Al_2O_3 were plotted against the CIA (Fig. 7a, 7b). The diagrams provide a basis for assessing increase or decrease in chemical mobility during progressive chemical weathering of the sediments in the Mekong River basin. The Na_2O pattern shows a strongly deceasing trend of chemical mobility ($r = -0.99$) rather than that of K_2O ($r = -0.64$), indicating a preferential hydrolysis of plagioclase (enrichment of Na) relative to K-feldspar and micas (enrichment in K) during the weathering process in the Mekong River basin. This is supported by a study of Liu et al. (2007) that also found higher alteration of plagioclase as compared to K-feldspar in Mekong River sediments.

4.2.2 CIA variability, chemical weathering and monsoon climate

Generally, warm temperature and abundant rainfall are the principal forcing factors for the chemical weathering on land in tropical Southeast Asia (Liu et al., 2012). Thus, a period of strengthening of the East Asian summer monsoon, which brings a humid climate and heavy rainfall in the basin (An et al., 2000; Liu et al., 2005, 2012; Colin et al., 2010), would be expected to increase CIA values following the basic principles of silicate weathering. Nevertheless, the general trend of CIA values recorded in Core SO18383-3 is not significantly correlated with East Asian paleomonsoon records, including stalagmite oxygen isotopes ($\delta^{18}O$) records of Hulu, Dongge, and northern Borneo caves (Wang et al., 2001; Dykoski et al., 2005; Carolin et al., 2016; Fig. 8). Accordingly, we believe that there is more complicated climate feedback than the summer monsoon intensity that effects the temporal variation of CIA values recorded in the studied core.

One possible reason for this is that the sediment grain size may influence the CIA variation, disturbing the significance as proxy of monsoon intensity or chemical weathering or both (e.g., Limmer et al., 2012a; Clift, 2015). Unfortunately, the grain size analysis does not coincide with

the geochemical analysis in this study. We tested the link with grain size using Al_2O_3/SiO_2 ratio since Al_2O_3 is mostly associated with clay minerals that is expected to be mostly controlled by the fine-grained sediment (Biscaye, 1965), whereas SiO_2 is contained particularly in quartz (SiO_2), commonly associated with the coarser-grained sediment fraction (Cuven et al., 2010). Thus, Al_2O_3/SiO_2 ratio is indicative of the relative proportion of aluminosilicates (fine-grained sediment) to quartz (coarse-grained sediment), and has been widely used as a grain size proxy (e.g., Calvert and Pedersen, 2007; Clift et al., 2014; Martinez-Ruiz et al., 2015). As shown in Figure 7c, CIA value displays a strong positive correlation with Al_2O_3/SiO_2 ratio ($r = 0.70$). This indicates that the temporal variation in CIA values recorded in Core SO18383-3 is significantly influenced by sediment grain size, and the greater CIA is primarily a result of the enrichment of fine-grained sediments in the weathering profile (Fig. 8). This evidence indicates that the variation in CIA value might be not sufficient to evaluate the instantaneous state of chemical weathering rates at specific monsoon rainfall conditions. This is in agreement with a previous study that has shown that the CIA probably cannot be used as a reliable proxy of instantaneous chemical weathering (Hu et al., 2012). Therefore, caution should be taken when using the temporal variation of CIA values as a proxy for reconstructing chemical weathering evolution from marine sedimentary records. However, on a long time scale, we observe CIA values of the last glacial period being lower than the Holocene ones (Fig. 8), reflecting stronger chemical weathering rate during the Holocene than during the LGM due to a strengthening of the Holocene summer monsoon (Wang and Wang, 1990; Wang et al., 1999; Hu et al., 2012). Related studies investigated the temporal variation of CIA values on longer time scales (million years) (e.g., Clift et al., 2008, 2014; Wei et al., 2006) but not on high-resolution millennial scales (e.g., Hu et al., 2012). Consequently, we conclude that the CIA recorded in the studied core can be a good indicator of the general weathering intensity registered in sediments with superimposed grain-size effects, which is sufficient to obtain a general picture of chemical weathering in the Mekong River basin, rather than modulations in the chemical weathering evolution.

4.2.3 Chemical weathering history using clay mineralogy and major element geochemistry

Although the temporal variation in the CIA value recorded in the studied core is less responsive to the continuous state of chemical weathering rate on a short-time scale, an alternative approach that can be used for reconstructing chemical weathering intensity is clay mineral compositions (e.g., Liu et al., 2004, 2005; Colin et al, 2010; Zhao, S. et al., 2018). In the Mekong River basin, clay minerals are produced by different processes and are distributed in different areas of the basin (Liu et al., 2004, 2005). Both illite and chlorite primarily result from the physical erosion of metamorphic and granitic rocks that are derived mainly from the eastern Tibetan Plateau, the hinterland of the Mekong River basin (Liu et al., 2005). Meanwhile, most of the kaolinite in this basin could also be derived from active erosion of inherited clays in the middle reach of the Mekong River (Liu et al., 2004). On the other hand, smectite is a secondary mineral that is mainly produced by chemical weathering of parent aluminosilicates and ferromagnesian silicates under warm and humid conditions in the lower part of the Mekong River basin (Liu et al., 2005). Therefore, smectite/(illite + chlorite) and smectite/kaolinite (Fig. 8) are employed as clay mineral proxies for reconstructing chemical weathering evolution in the Mekong River basin (e.g., Liu et al., 2004, 2005; Colin et al., 2010).

Considering major element geochemistry, TiO_2/K_2O ratio can be applied as an elemental proxy for chemical weathering, which has been investigated to reconstruct the chemical weathering in previous studies (e.g., Wei et al., 2003; Bastian et al., 2017). TiO_2 is extremely resistant to weathering (Nesbitt and Young, 1982; Wei et al., 2003) and is incorporated into secondary minerals, including clays in marine sediments (Zhang et al., 2002; Bastian et al., 2017). In contrast, K_2O is highly mobile during weathering processes, and hence is usually depleted in chemically weathered sediments (Nesbitt et al., 1980; Condie et al., 1995). Hence, the TiO_2/K_2O ratio is employed as elemental proxy for reconstructing chemical weathering intensity in the source area. However, it is noted that this elemental proxy may also be influenced by variations in grain size. We assess the possible role of grain size by comparing

with Al_2O_3/SiO_2 ratio (Fig. 7d). The lack of significant correlation between Al_2O_3/SiO_2 and TiO_2/K_2O ratios (r = 0.08, Fig. 7d)–indicates that the TiO_2/K_2O ratio of the studied core is not significantly affected by grain size variation. Therefore, we propose that the variation in TiO_2/K_2O ratio does express variations in chemical weathering in the Mekong River basin.

It is noted that sea level change can affect variations in terrigenous sediment input to the southern SCS basin (Steinke et al., 2003; Jiwarungrueangkul et al., 2019), which may cause variations of these clay mineral and elemental proxies. In the southern SCS, major sea level rise of about 40 m occurred at ~14.5 cal ka BP during the meltwater pulse (MWP) 1A, leading to a sudden retreat of paleo-river mouths toward the land and flooding of the exposed shelf (Jiwarungrueangkul et al., 2019; Fig. 1). Since the characteristic of the shelf at the paleo-Mekong River mouth is high-gradient and very narrow morphology (Fig. 1), it could have retreated slowly on the continental shelf during the MWP-1A (Tjallingii et al., 2010). A rapid migration of the paleo-Mekong River mouth could have occurred during the accelerated rate of sea level rise (~25 mm/yr) between 9.5 and 8.5 cal ka BP rising from about 34 to 9 m below modern sea level corresponding to the sea-level jump of the MWP-1C (Fig. 8; Tjallingii et al., 2010). Considering with our proxies, the most prominent changes in smectite/(illite + chlorite), smectite/ kaolinite, and TiO_2/K_2O ratios occurred prior to the major morphology modification of shelf off the Mekong River at the MWP-1C (Fig. 8), implying that sea level change may not have significantly affected the variations in these proxies. Besides, a short sediment transport distance between the core location and the Mekong River mouth may be largely unaffected by glacio-eustasy of clay mineral variations (e.g., Liu et al., 2010). This emphasizes that smectite/(illite + chlorite), smectite/kaolinite, and TiO_2/K_2O ratios can employ to reconstruct chemical weathering evolution.

In Core SO18383-3, the temporal variations in smectite/(illite + chlorite), smectite/kaolinite, and TiO_2/K_2O ratios show similar changes over the last 29.9 ka (Fig. 8). In comparison with the stalagmite $\delta^{18}O$ records, three main periods of chemical weathering evolution within the Mekong River basin likely coincide with the pattern variations of the Chinese stalagmite $\delta^{18}O$

rather than the northern Borneo stalagmite $\delta^{18}O$ records (Fig. 8). This may reveal significant controlling factor of chemical weathering evolution within the Mekong River basin. Seeing that hydrological cycle in the northern Borneo since the LGM is generally associated by the Warm Pool convective activity (El Niño-Southern Oscillation; Partin et al., 2007) while in China is dominated by the East Asian summer monsoon. Therefore, it can be considered that chemical weathering within the Mekong River basin over the last 29.9 ka responses to the prevailing East Asian summer monsoon.

During the period around LGM (29.9–14.7 cal ka BP), the sediments in Mekong River basin are characterized to have experienced weak chemical weathering inferred from the relatively lower values of three proxies (Fig. 8). The weak chemical weathering during this period is related well to the weakening of the East Asian summer monsoon inferred from the Chinese stalagmite $\delta^{18}O$ records (Wang et al., 2001; Dykoski et al., 2005; Fig. 8). This indicates that lower chemical weathering intensity in the Mekong River basin during the LGM period was caused by a weakened summer monsoon. During an abrupt climate change in this period, the Chinese stalagmite records show a rapid change to heavy $\delta^{18}O$ value, implying an abrupt decrease in the East Asian summer monsoon intensity (Wang et al., 2001; Dykoski et al., 2005). However, change in chemical weathering intensity recorded by the studied core is not evident during the Heinrich Event 2. This may be explained the Heinrich Event 2 possibly occurred with short duration (Fig. 8), which cannot lead to change the chemical weathering intensity within the Mekong River basin due to the longer time period required for the chemical weathering processes. Also, some uncertainty of our age model obtained by linear interpolation between dating points (Fig. 2) cannot be excluded. Even so, we observe the weakest chemical weathering during this period coinciding with long periods of the Heinrich Event 1 (~14.8 cal ka BP) when the most weakening of the East Asian summer monsoon occurred in this region (Fig. 8; Wang et al., 2001; Dykoski et al., 2005).

During the main deglaciation period (14.7–7.6 cal ka BP), increases in values of these proxies imply that the sediments in the Mekong River basin evidence an increasing chemical

weathering intensity compared to the previous period. This coincides with the increase in the East Asian summer monsoon intensity (Fig. 8); thus, we suggest that an increase in chemical weathering intensity during the main deglaciation period was the result of a strengthening of the summer monsoon rainfall during this period.

A rapid increase in chemical weathering intensity in the Mekong River basin during this period is observed during 14.7–12.7 cal ka PB, which is well aligned with the Bølling-Allerød interstadial (Fig. 8). The climate during the Bølling-Allerød period appears an abrupt warm and strengthening of East Asian summer monsoon (Wang et al., 2001; Stebich et al., 2009; Li et al., 2011). Additionally, a significant decrease in chemical weathering in the Mekong River basin is observed between 12.4 and 11.3 cal ka BP. This phenomenon is associated with a cooling in the areas around mainland Asia (Sun et al., 2005; Zhao et al., 2006), which is related to an interval of a weakened summer monsoon intensity (Wang et al., 2001; Dykoski et al., 2005; Fig. 8) as effect of the Younger Dryas cold period (Stuiver et al., 1995). This general pattern of the Younger Dryas agrees with the changes in pollen records from the Tiancia Lake in southwestern China (Xiao et al., 2014) and from the Huguangyan Maar Lake in southern China (Sheng et al., 2017), reflecting the impact of a decrease in summer monsoon precipitation during the Younger Dryas. Overall, our findings provide evidence of chemical weathering response to rapid climate change during the Bølling-Allerød and Younger Dryas periods. During the mid to late Holocene (7.6–1.1 cal ka BP), the Mekong River basin was subject to a progressive decrease of chemical weathering intensity as indicated by the gradual decrease in values of the weathering proxies (Fig. 8). A slight decrease in chemical weathering in this time interval corresponds to a weakening of the East Asian summer monsoon (Maher, 2008; Fig. 8). This implies that the decrease in the chemical weathering intensity in the Mekong River basin is due to a weakened summer monsoon in this time interval.

Our findings exhibit clearly that the variation in chemical weathering intensity in the Mekong River basin since 29.9 cal ka BP has been strongly related to the East Asian summer monsoon evolution. A weaker chemical weathering intensity can be observed in the periods around the

LGM (29.9–14.7 cal ka BP) and mid to late Holocene (7.6–1.1 cal ka BP), as well as during abrupt climate change periods in the Heinrich Event 1 (~14.8 cal ka BP) and Younger Dryas cooling (12.4–11.3 cal ka BP), when the East Asian summer monsoon weakens. This is possibly also associated with changes in the vegetation cover within the basin. In general, the vegetation development around mainland Asia was promoted by significantly increased summer monsoon rainfall (Zhang et al., 2016; Wen et al., 2017); thus, the period of a weakened monsoon rainfall would be expected to decrease the vegetation cover in the Mekong River basin. This could lead to a predominance of detrital material issued from the physical erosion (illite, chlorite, and kaolinite) (Liu et al., 2004) and thus to a lower input of chemically weathered sediment supplied by the river during a weakening of the East Asian summer monsoon. In contrast, a strengthened chemical weathering intensity is found during the main deglaciation period (14.7–7.6 cal ka BP) and an accelerated increase in chemical weathering intensity is at the Bølling-Allerød period (14.7–12.7 cal ka BP), when the summer monsoon increased (Fig. 8). During wet and warm period of summer monsoon reinforcement, the vegetation cover could increase in the Mekong River basin. This cover promotes soil development and thus the production and supply of chemically weathered sediments (smectite) during a strengthening of the East Asian summer monsoon.

For further considering the depth-related chemical weathering variation signals preserved by clay mineralogy off the Mekong River mouth, the ratios of smectite/(illite + chlorite) and smectite/kaolinite of a neighboring Core MD01-2393 from the continental slope along the Mekong River at 1,230 m water depth (Liu et al., 2004; Fig. 1) is compared with those of Core SO18383-3. The results show that temporal variations of clay mineral ratios of Core SO18383-3 are similarly to those of Core MD01-2393 (Fig. 8), suggesting that the variation in clay mineral compositions off the Mekong River mouth since the LGM mainly reflects the evaluation of chemical weathering intensity within the Mekong River basin. Except for the interval of 4.5 to 1.1 cal ka BP, relatively higher smectite/(illite + chlorite) and smectite/kaolinite are encountered in Core MD01-2393 (deeper water core), comparing with lower values in Core

SO18383-3 (shallow water core). It could result from the differential settling effect of smectite when the deeper core location was farther from the Mekong River mouth during the Holocene sea level stand (Fig. 1; Ta et al., 2002).

Our discussion primarily reveals an influence of the East Asian summer monsoon on chemical weathering; however, several previous studies have mentioned a decoupling of chemical weathering and the East Asian summer monsoon. For example, studies of elemental and clay mineral proxies in the Taiwan orogeny have found that an intensification of the East Asian summer monsoon may limit chemical weathering rates as erosion rates increase, soil residence times decrease, and weatherable minerals do not have sufficient time for chemical weathering reactions (Dadson et al., 2003; Zhao et al., 2017). Furthermore, Dosseto et al. (2015) investigated the weathering records by using δ^7Li variations in clay fraction in the Himalayan range, suggesting that a significant increase in erosion rates is linked to a strengthening of the Indian summer monsoon rainfall since the end of the LGM, mainly via increased runoff and its effect on land sliding or fluvial incision or both. Those regions characterized by tectonically active mountainous catchment are quite different from the Mekong River basin. The landscape of the Mekong River basin, especially in the middle-lower reaches, is characterized by tectonically stable river basin and broad alluvial plain (Liu et al., 2004). We suggest that tectonic activity is no major controlling factor on silicate weathering in the Mekong River basin. This agrees with findings from the Irrawaddy floodplain in Southeast Asia showing an increase in the chemical weathering related to the stronger summer monsoon rainfall (Colin et al., 2006).

4. Conclusions

Clay mineralogy and major element geochemistry from Core SO18383-3 in the southern SCS were investigated to examine the detailed records of provenance and chemical weathering intensity in the Mekong River basin since 29.9 cal ka BP. The major conclusions are as follows:

(1) Clay mineral analysis for Core SO18383-3 suggests that the Mekong River is the major sediment supplier for this area located off the Mekong River.

(2) The CIA values recorded in core sediments range from 71 to 77 (average 73), referring to moderate weathering in the Mekong River basin over the last 29.9 ka.

(3) Chemical weathering evolution in the Mekong River basin is mainly controlled by the change in the East Asian summer monsoon intensity. A weakening of the summer monsoon around the LGM (29.9–14.7 cal ka BP), the Heinrich Event 1 (~14.8 cal ka BP), the Younger Dryas interval (12.4-11.3 cal ka BP), and mid to late Holocene (7.6–1.1 cal ka BP) led to a decrease of the chemical weathering intensity in the Mekong River basin. In contrast, a strengthening of summer monsoon during the main deglaciation period (14.7–7.6 cal ka BP) and the Bølling-Allerød period (14.7–12.7 cal ka BP) resulted in an increase of chemical weathering intensity in the Mekong River basin.

Acknowledgments

We would like to thank the crew and scientists on board the R/V *SONNE* for collecting sediment cores during cruise SO-140 in 1999. We also thank Dr. Jan Scholten from Institute of Geosciences, University of Kiel for sub-sampling and Dr. Yanli Li from State Key Laboratory of Marine Geology, Tongji University for laboratory assistance. This work was supported by the National Key R&D Program of China (2018YFE0202402), the Second Tibetan Plateau Scientific Expedition and Research (STEP) Program (SQ2019QZKK2304), and the National Natural Science Foundation of China (41530964). Data generated by this study are available at the PANGAEA database (https://doi.pangaea.de/10.1594/PANGAEA.905089).

References

An, Z., Porter, S.C., Kutzbach, J.E., Wu, X., Wang, S., Liu, X., et al. (2000). Asynchronous Holocene optimum of the East Asian monsoon. *Quaternary Science Reviews, 19,* 743–762.

Bastian, L., Revel, M., Bayon, G., Dufour, A., & Vigier, N. (2017). Abrupt response of chemical

weathering to Late Quaternary hydroclimate changes in northeast Africa. *Scientific Reports, 7,* doi:10.1038/srep44231.

Biscaye, P.E. (1965). Mineralogy and sedimentation of recent deep-sea clays in the Atlantic Ocean and adjacent seas and oceans. *Geological Society of America Bulletin,* 76, 803–832.

Blaauw, M., & Christen, J.A. (2011). Flexible paleoclimate age-depth models using an autoregressive gamma process. *Bayesian Analysis,* 6, 457–474.

Calvert, S.E., & Pedersen, T.F. (2007). Elemental Proxies for Palaeoclimatic and Palae oceanographic Variability in Marine Sediments: Interpretation and Application, In: Hillaire–Marcel, C. and De Vernal, A. (Eds), Proxies in Late Cenozoic Paleoceanography. Elsevier, Netherlands, pp. 567–644.

Carolin, S.A., Cobb, K.M., Lynch-Stieglitz, J., Moerman, J.W., Partin, J.W., & Lejau, S., et al. (2016). Northern Borneo stalagmite records reveal West Pacific hydroclimate across MIS 5 and 6. *Earth and Planetary Science Letters,* 439, 182–193.

Chamley, H. (1989). Clay Sedimentology. Springer-Verlag, New York.

Chen, Q., Liu, Z., & Kissel, C. (2017). Clay mineralogical and geochemical proxies of the East Asian summer monsoon evolution in the South China Sea during Late Quaternary. *Scientific Reports, 7,* doi:10.1038/srep42083.

Clift, P.D. (2015). Assessing effective provenance methods for fluvial sediment in the South China Sea, In: Clift, P.D., Harff, J., Wu, J., Qui, Y. (Eds.), River-Dominated Shelf Sediments of East Asian Seas. Geological Society of London (Special Publication 429), London, pp. 9–29.

Clift, P.D., Layne, G.D., & Blusztajn, J. (2004). Marine sedimentary evidence for monsoon strengthening, Tibetan uplift and drainage evolution in East Asian, in Continent Ocean Interactions Within East Asian Marginal Seas. *Geophysical Monograph Series, 149,* 255–282.

Clift, P.D., Hodges, K.V., Heslop, D., Habbigan, R., Hoang, L.V., & Calves, G. (2008). Greater Himalayan exhumation triggered by Early Miocene monsoon intensification. *Nature*

Geoscience, 1, 875–880.

Clift, P.D., Wan, S., & Blusztajn, J. (2014). Reconstructing chemical weathering, physical erosion and monsoon intensity since 25 Ma in the northern South China Sea: A review of competing proxies. *Earth-Science Reviews, 130,* 86–102.

Colin, C., Siani, G., Sicre, M.-A., & Liu, Z. (2010). Impact of the East Asian monsoon rainfall changes on the erosion of the Mekong River basin over the past 25,000 yr. *Marine Geology, 271,* 84–92.

Colin, C., Turpin, L., Blamart, D., Frank, N., Kissel, C., & Duchamp, S. (2006). Evolution of weathering patterns in the Indo-Burman Ranges over the last 280 kyr: Effects of sediment provenance on $^{87}Sr/^{86}Sr$ ratios tracer. *Geochemistry, Geophysics, Geosystems, 7*, Q03007, doi:10.1029/2005GC000962.

Condie, K., Dengate, J., & Cullers, R. (1995). Behavior of rare earth elements in a paleoweathering profile on granodiorite in the Front Range, Colorado, USA. *Geochimica et Cosmochimica Acta, 59,* 279–294.

Cuven, S., Francus, P., & Lamoureux, S.F. (2010). Estimation of grain size variability with micro X-ray fluorescence in laminated lacustrine sediments, Cape Bounty, Canadian High Arctic. *Journal of Paleolimnology, 44,* 803–817.

Dadson, S., Hovius, N., Chen, H., Dade, W., Hsieh, M., Willett, S., et al. (2003). Links between erosion, runoff variability and seismicity in the Taiwan orogen. *Nature, 426 (6967),* 648–651.

Debenay, J.P., & Luan, B.T. (2006). Foraminiferal assemblages and the confinement index as tools for assessment of saline intrusion and human impact in the Mekong Delta and neighboring areas (Vietnam). *Rev Micropaléontol, 49,* 74–85.

Dosseto, A., Vigier, N., Joannes-Boyau, R., Moffat, I., Singh, T., & Srivastava, P. (2015). Rapid response of silicate weathering rates to climate change in the Himalaya. *Geochemical Perspectives Letters, 1,* 10–19.

Dykoski, C.A., Edwards, R.L., Cheng, H., Yuan, D., Cai, Y., Zhang, M., et al. (2005). A high-resolution, absolute-dated Holocene and deglacial Asian monsoon record from Dongge

Cave, China. *Earth and Planetary Science Letters, 233,* 71–86.

Esquevin, J. (1969). Influence de la composition chimique des illites sur leur cristallinité. Bull. Centre Rech. Pau-SNPA.

Fu, S., Zhu, Z., Ouyang, T., Qiu, Y., & Wei, Z. (2011). Geochemical changes of the terrigenous sediments in the southern South China Sea and their paleoenvironmental implications during the last 31 ky. *Journal Of Oceanography, 67,* 337–346.

Hanebuth, T.J.J., Stattegger, K., & Grootes, P.M. (2000). Rapid flooding of the Sunda Shelf: A late-glacial sea-level record. *Science,* 288, 1033–1035.

Hanebuth, T.J.J., Voris, H.K., Yokoyama, Y., Saito, Y., & Okuno, J. (2011). Formation and fate of sedimentary depocentres on Southeast Asia's Sunda Shelf over the past sea-level cycle and biogeographic implications. *Earth-Science Reviews, 104,* 92–110.

Holtzapffel, T. (1985). Les minéraux argileux: préparation, analyse diffractométrique et determination. *Society Géological Nord Publication, 12,* 1–136.

Hu, D., Böning, P., Köhler, C.M., Hillier, S., Pressling, N., Wan, S., et al. (2012). Deep sea records of the continental weathering and erosion response to East Asian monsoon intensification since 14 ka in the South China Sea. *Chemical Geology, 326–327,* 1–18.

Hu, J., Peng, P., Fang, D., Jia, G., Jian, Z., & Wang, P. (2003). No aridity in Sunda Land during the Last Glaciation: Evidence from molecular-isotopic stratigraphy of long-chain n-alkanes. P*alaeogeography, Palaeoclimatology, Palaeoecology, 201,* 269–281.

Huang, J., Jiang, F., Wan, S., Zhang, J., Li, A., & Li, T. (2016). Terrigenous supplies variability over the past 22,000yr in the southern South China Sea slope: Relation to sea level and monsoon rainfall changes. *Journal of Asian Earth Sciences, 117,* 317–327.

Jiwarungrueangkul, T., Liu, Z., & Zhao, Y. (2019). Terrigenous sediment input responding to sea level change and East Asian monsoon evolution since the last deglaciation in the southern South China Sea. *Global and Planetary Change,* 174, 127-137.

Lambeck, K., Rouby, H., Purcell, A., Sun, Y., & Sambridg, M. (2014). Sea level and global ice volumes from the Last Glacial Maximum to the Holocene. *Proceedings of the National Academy of Sciences of the United States of America,* 111, 15296–15303.

Li, C., Wu, Y., & Hou, X. (2011). Holocene vegetation and climate in Northeast China revealed from Jingbo Lake sediment. *Quaternary International, 229*, 67–73.

Li, Q., Zheng, F., Chen, M., Xiang, R., Qiao, P., Shao, L., et al. (2010). Glacial paleoceanography off the mouth of the Mekong River, southern South China Sea, during the last 500 ka. *Quaternary Research*, 73, 563–572.

Libes, S.M. (2009). Introduction to Marine Biogeochemistry. Elsevier, Academic Press, 909 pp. doi:10.1016/0304-4203(93)90016-H.

Limmer, D.R., Böning, P., Giosan, L., Ponton, C., Köhler, C.M., Cooper, M.J., et al. (2012a). Geochemical record of Holocene to recent sedimentation on the western Indus continental shelf, Arabian Sea. *Geochemistry, Geophysics, Geosystems, 13,* Q01008, doi:10.1029/ 2011GC003845.

Limmer, D.R., Köhler, C.M., Hiller, S., Moreton, S.G., Tabrez, A.R., & Clift, P.D. (2012b). Chemical weathering and provenance evolution of Holocene-recent sediments from the western Indus Shelf, northern Arabian Sea inferred from physical and mineralogical properties. *Marine Geology, 326–328,* 101–115.

Liu, Z., Colin, C., Huang, W., Le, K.P., Tong, S., Chen, Z., et al. (2007). Climatic and tectonic controls on weathering in south China and Indochina Peninsula: Clay mineralogical and geochemical investigations from the Pearl, Red, and Mekong drainage basins. *Geochemistry, Geophysics, Geosystems, 8,* Q05005, doi:10.1029/2006GC001490.

Liu, Z., Colin, C., Trentesaux, A., Blamart, D., Bassinot, F., Siani, G., et al. (2004). Erosional history of the eastern Tibetan Plateau since 190 kyr ago: Clay mineralogical and geochemical investigations from the southwestern South China Sea. *Marine Geology, 209,* 1–18.

Liu, Z., Colin, C., Trentesaux, A., Siani, G., Frank, N., Blamart, D., et al. (2005). Late Quaternary climatic control on erosion and weathering in the eastern Tibetan Plateau and the Mekong Basin. *Quaternary Research, 63,* 316–328.

Liu, Z., & Stattegger, K. (2014). South China Sea fluvial sediments: An introduction. *Journal of Asian Earth Sciences, 79,* 507–508.

Liu, Z., Wang, H., Hantoro, W.S., Sathiamurthy, E., Colin, C., Zhao, Y., et al. (2012). Climatic and tectonic controls on chemical weathering in tropical Southeast Asia (Malay Peninsula, Borneo, and Sumatra). *Chemical Geology, 291,* 1–12.

Liu, Z., Zhao, Y., Colin, C., Stattegger, K., Wiesner, M.G., Huh, C.-A., et al. (2016). Source-to-sink transport processes of fluvial sediments in the South China Sea. E*arth-Science Reviews, 153,* 238–273.

Ludwig, W., Amiotte-Suchet, P., & Probst, J.L. (1999). Enhanced chemical weathering of rocks during the last glacial maximum: a sink for atmospheric CO_2?. *Chemical Geology, 159,* 147–161.

Maher, B.A. (2008). Holocene variability of the East Asiansummer monsoon from Chinese caverecords: a re-assessment. *The Holocene, 18*, 861–866.

Martinez-Ruiz, F., Kastner, M., Gallego-Torres, D., Rodrigo-Gamiz, M., Nieto-Moreno, V., & Ortega-Huertas, M. (2015). Paleoclimate and paleoceanography over the past 20,000 yr in the Mediterranean Sea Basins as indicated by sediment elemental proxies. *Quaternary Science Reviews, 107,* 25–46.

Meybeck, M. (1987). Global chemical weathering of surficial rocks estimated from river dissolved loads. *American Journal of Science, 287,* 401–428.

Milliman, J.D., Farnsworth, K.L., & Albertin, C.S. (1999). Flux and fate of fluvial sediments leaving large islands in the East Indies. *Journal of Sea Research, 41,* 97–107.

Milliman, J.D., & Syvitski, J.P.M. (1992). Geomorphic/Tectonic Control of Sediment Discharge to the Ocean: The Importance of Small Mountainous Rivers. *Journal of Geology, 100,* 525–544.

Miriyala, P., Sukumaran, N.P., Nagender Nath, B., Ramamurty, PB., Sijinkumar, A.V., Vijayagopal, B., Ramaswamy, V. & Sebastian, T. (2017). Increased chemical weathering during the deglacial to mid-Holocene summer monsoon intensification. *Scientific Reports*, 7, 44310; doi: 10.1038/srep44310.

Nesbitt, H., Markovics, G., & Price, R. (1980). Chemical processes affecting alkalis and alkaline earths during continental weathering. *Geochimica et Cosmochimica Acta, 44,*

1659–1666.

Nesbitt, H., & Young, G.M. (1982). Early Proterozoic climates and plate motions inferred from major element chemistry of lutites. *Nature, 299,* 715–717.

Oliva, P., Viers, J., & Dupre, B. (2003). Chemical weathering in granitic environments. *Chemical Geology, 202,* 225–256.

Partin, J.W., Cobb, K.M., Adkins, J.F., Clark, B., & Fernandez, D.P. (2007). Millennial-scale trends in west Pacific warm pool hydrology since the Last Glacial Maximum. *Nature, 449*, 452–453.

Reimer, P.J., Bard, E., Bayliss, A., Beck, J.W., Blackwell, P.G., Bronk Ramsey, C., et al. (2013). IntCal13 and Marine13 Radiocarbon Age Calibration Curves 0–50,000 Years cal BP. *Radiocarbon, 55,* 1869–1887.

Riebe, C.S., Kirchner, J.W., & Finkel, R.C. (2004). Erosional and climatic effects on long-term chemical weathering rates in granitic landscapes spanning diverse climate regimes. *Earth and Planetary Science Letters, 224,* 547–562.

Sathiamurthy, E., & Voris, K.H. (2006). Maps of Holocene Sea Level Transgression and Submerged Lakes on the Sunda Shelf. *The Natural History Journal of Chulalongkorn University, Supplement, 2,* 1–44.

Sheng, M., Wang, X., Zhang, S., Chu, G., Su, Y., & Yang, Z. (2017). A 20,000-year high-resolution pollen record from Huguangyan Maar Lake in tropical–subtropical South China. *Palaeogeography, Palaeoclimatology, Palaeoecology, 472,* 83–92.

Stebich, M., Mingram, J., Han, J., & Liu, J. (2009). Late Pleistocene spread of (cool-) temperate forests in Northeast China and climate changes synchronous with the North Atlantic region. *Global and Planetary Change, 65,* 56–70.

Steinke, S., Hanebuth, T.J.J., Vogt, C., & Stattegger, K. (2008). Sea level induced variations in clay mineral composition in the southwestern South China Sea over the past 17,000 yr. *Marine Geology, 250,* 199–210.

Steinke, S., Kienast, M., & Hanebuth, T.J.J. (2003). On the significance of sea-level variations and shelf paleo-morphology in governing sedimentation in the southern South China Sea

during the last deglaciation. *Marine Geology,* 201, 179–206.

Stuiver, M., Grootes, P.M., & Braziunas, T.F. (1995). The GISP2 $N^{18}O$ climate record of the past 16,500 years and the role of the Sun, ocean, and volcanoes. *Quaternary Research, 44,* 341–354.

Sun, Y., Oppo, D.W., Xiang, R., Liu, W., & Gao, S. (2005). Last deglaciation in the Okinawa Trough: Subtropical northwest Pacific link to Northern Hemisphere and tropical climate. *Paleoceanography, 20,* PA4005. doi:10.1029/2004PA001061.

Ta, T.K.O., Nguyen, V.L., Tateishi, M., Kobayashi, I., Tanabe, S., & Saito, Y. (2002). Holocene delta evolution and sediment discharge of the Mekong River, southern Vietnam. *Quaternary Science Reviews, 21,* 1807 – 1819.

Tamura, T., Saito, Y., Sieng, S., Ben, B., Kong, M., Sim, I., Choup, S., Akiba, F., 2009. Initiation of the Mekong River delta at 8 ka: evidence from the sedimentary succession in the Cambodian lowland. *Quaternary Science Reviews, 28 (3–4)*, 327–344.

Taylor, S.R., & McLennan, S.M. (1985). The Continental Crust: Its Composition and Evolution. Blackwell Scientific, Oxford.

Tjallingii, R., Stattegger, K., Stocchi, P., Saito, Y., & Wetzel, A. (2014). Rapid flooding of the southern Vietnam shelf during the early to mid-Holocene. *Journal of Quaternary Science,* 29, 581–588.

Tjallingii, R., Stattegger, K., Wetzel, A., & Van Pach, P. (2010). Infilling and flooding of the Mekong River incised-valley system during deglacial sea-level rise. *Quaternary Science Reviews,* 29, 1432-1444.

Unverricht, D., Szczuciński, W., Stattegger, K., Jagodziński, R., Le, X.T., & Kwong, L.L.W. (2013). Modern sedimentation and morphology of the subaqueous Mekong Delta, Southern Vietnam. *Global and Planetary Change, 110, B,* 223–235.

Voris, H.K., 2000. Maps of Pleistocene sea levels in Southeast Asia: Shorelines, river systems and time durations. *Journal of Biogeography, 27,* 1153–1167.

Wan, S., Clift, P.D., Zhao, D., Hovius, N., Munhoven, G., France-Lanord, C., et al. (2017). Enhanced silicate weathering of tropical shelf sediments exposed during glacial

lowstands: A sink for atmospheric CO_2. *Geochimica et Cosmochimica Acta, 200,* 123–144.

Wan, S., & Jian Z. (2014). Deep water exchanges between the South China Sea and the Pacific since the last glacial period. *Paleoceanograpgy*, 29, 1160–1178.

Wan, S., Tian, J., Steinke, S., Li, A., & Li, T. (2010). Evolution and variability of the East Asian summer monsoon during the Pliocene: Evidence from clay mineral records of the South China Sea. *Palaeogeography, Palaeoclimatology, Palaeoecology, 293,* 237–247.

Wang, J., Li, A., Xu, K., Zheng, X., & Huang, J. (2015). Clay mineral and grain size studies of sediment provenances and paleoenvironment evolution in the middle Okinawa Trough since 17 ka. *Marine Geology, 366,* 49–61.

Wang, L., Sarnthein, M., Erlenkeuser, H., Grimalt, J., Grootes, P., Heilig, S., et al. (1999). East Asian monsoon climate during the Late Pleistocene: high-resolution sediment records from the South China Sea. *Marine Geology, 156,* 245–284.

Wang, L., & Wang, P. (1990). Late Quaternary paleoceanography of the South China Sea: glacial-interglacial contrasts in an enclosed basin. *Paleoceanography, 5,* 77–90.

Wang, Y., Cheng, H., Edwards, R.L., An, Z.S., Wu, J.Y., Shen, C.C., et al. (2001). A High-Resolution Absolute-Dated Late Pleistocene Monsoon Record from Hulu Cave, China. *Science, 294,* 2344–2348.

Wehausen, R., Tian, J., Brumsack, H., Cheng, X., & Wang, P. (2003). Geochemistry of Pliocene Sediments from ODP Site 1143 (Southern South China Sea). *Proceedings of the Ocean Drilling Program Scientific Results, 184,* 1–25.

Wei, G., Li, X., Liu, Y., Shao, L., & Liang, X. (2006). Geochemical record of chemical weathering and monsoon climate change since the early Miocene in the South China Sea. *Paleoceanography, 21,* 1–11.

Wei, G., Liu, Y., Li, X., Shao, L., & Liang, X. (2003). Climatic impact on Al, K, Sc and Ti in marine sediments: Evidence from ODP Site 1144, South China Sea. *Geochemical Journal, 37,* 593–602.

Wen, R., Xiao, J., Fan, J., Zhang, S., & Yamagata, H. (2017). Pollen evidence for a mid-

Holocene East Asian summer monsoon maximum in northern China. *Quaternary Science Reviews, 176,* 29–35.

Xiao, X., Haberle, S. G., Shen, J., Yang, X., Han, Y., Zhang, E., et al. (2014). Latest Pleistocene and Holocene vegetation and climate history inferred from an alpine lacustrine record, northwestern Yunnan Province, southwestern China. *Quaternary Science reviews, 86,* 35–48.

Xue, Z., He, R., Liu, J.P. & Warner, J.C. (2012). Modeling transport and deposition of the Mekong River sediment. *Continental Shelf Research, 37,* 66–78.

Zhang, C., Wang, L., Li, G., Dong, S., Yang, J., & Wang, X. (2002). Grain size effect on multi-element concentrations in sediments from the intertidal flats of Bohai Bay, China. *Applied Geochemistry, 17,* 59–68.

Zhang, E., Wang, Y., Sun, W., & Shen, J., 2016. Holocene Asian monsoon evolution revealed by a pollen record from an alpine lake on the southeastern margin of the Qinghai–Tibetan Plateau, China. *Climate of the Past, 12,* 415–427.

Zhao, D., Wan, S., Clift, P.D., Tada, R., Huang, J., Yin, X., et al. (2018). Provenance, sea-level and monsoon climate controls on silicate weathering of Yellow River sediment in the northern Okinawa Trough during late last glaciation. *Palaeogeography, Palaeoclimatology, Palaeoecology, 490,* 227–239.

Zhao, S., Liu, Z., Colin, C., Zhao, Y., Wang, X., & Jian, Z. (2018). Responses the East Asian summer monsoon in the low-latitude South China Sea to high-latitude millennial-scale climatic changes during the last glaciation: Evidence from a high-resolution clay mineralogical record. *Paleoceanography and Paleoclimatology, 33*. https://doi.org/10. 1029/2017PA003 235

Zhao, M., Huang, C.Y., Wang, C.C., & Wei, G.A. (2006). Millennial-scale U_{37}^{K} sea-surface temperature record from the South China Sea (8°N) over the last 150 kyr: Monsoon and sea-level influence. *Palaeogeography, Palaeoclimatology, Palaeoecology, 236,* 39–55.

Zhao, Y., Yang, S., Liu, J., Fan, D., Yang, R., Bi, L., et al. (2017). Reconstruction of silicate

weathering intensity and paleoenvironmental change during the late Quaternary in the Zhuoshui River catchment in Taiwan. *Quaternary International, 452,* 43–53.

Table 1 AMS ^{14}C dating of Core SO18383-3 in the southwestern South China Sea.

Depth (cm)	Sample depth (cm)	Sample material	Radiocarbon age (yr BP)	Calibrated age (cal yr BP)
4-13	8.5	*G. ruber*	1,710±30	1,291±127 (1,180–1,434)
96-97	96.5	*G. ruber*	6,750±30	7,306±136 (7,161–7,433)
172-181	176.5	*G. ruber*	9,620±30	10,446±251 (10,140–10,641)
208-217	212.5	*G. ruber*	9,680±30	10,795±253 (10,600–11,107)
424-433	428.5	Mixed foraminifera*	13,220±40	15,372±339 (15,072–15,751)
936-937	936.5	Mixed foraminifera*	26,060±100	29,852±645 (29,189–30,432)

*Mixed benthic and planktic foraminifera for radiocarbon dating.

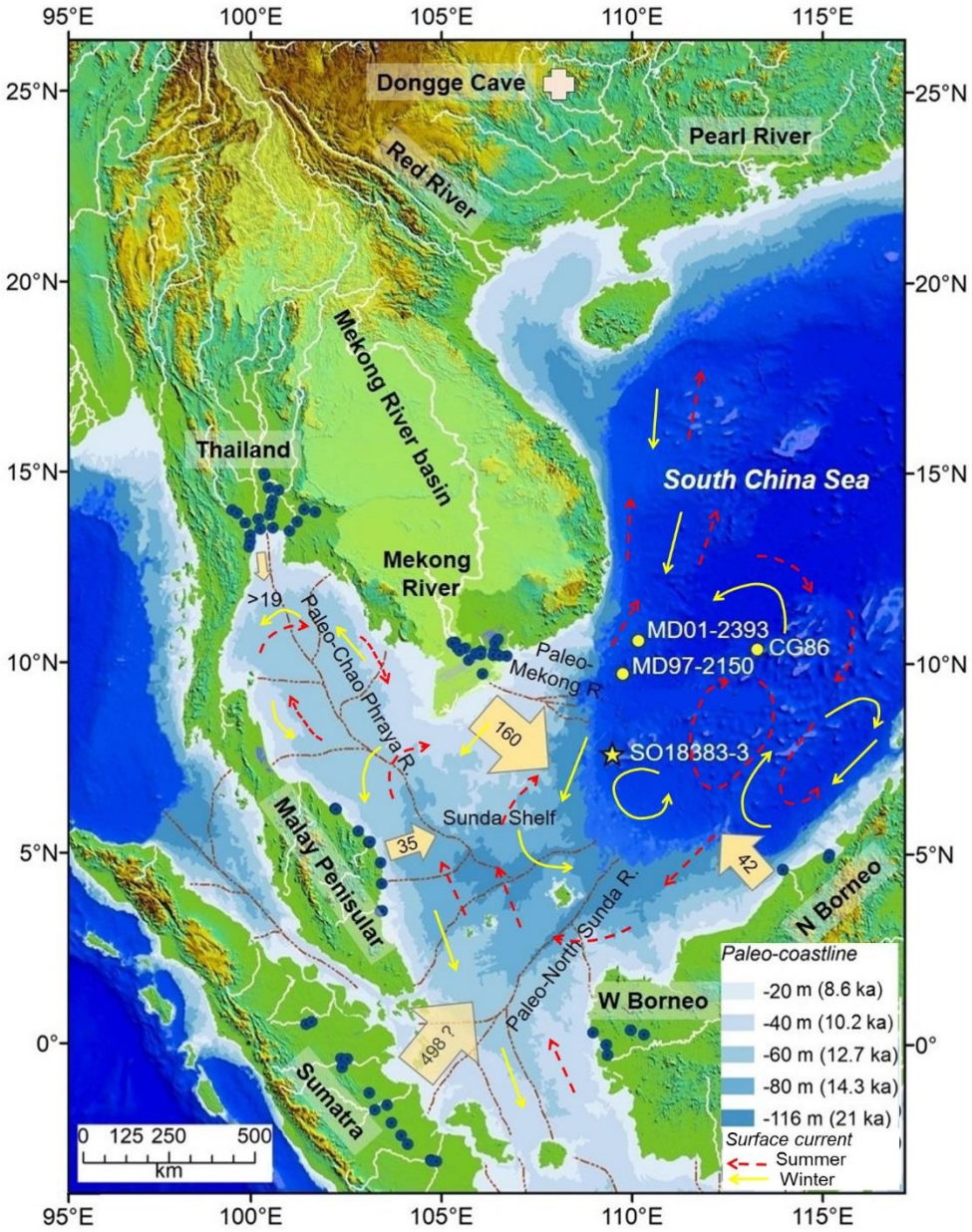

Figure 1. Topographic map of SE Asia showing modern fluvial drainage systems surrounding the South China Sea (SCS) and paleo-river systems developed on the Sunda Shelf during the LGM sea-level lowstand. The locations of Core SO18383-3 (yellow star) and referred cores (yellow circles) and river samples (blue circles) used in this paper are presented. Arrows with numbers indicate annual suspended sediment discharge (Mt/yr) (revised after Liu and Stattegger, 2014). Arrow lines show surface current systems in winter (yellow) and summer (red), which are after Liu et al., 2016). Paleo-coastlines are based on present-day bathymetric depth contours (Hanebuth et al., 2011; Tjallingii et al., 2014). Paleo-river systems are modified from Voris (2000) and Sathiammurthy and Voris (2006).

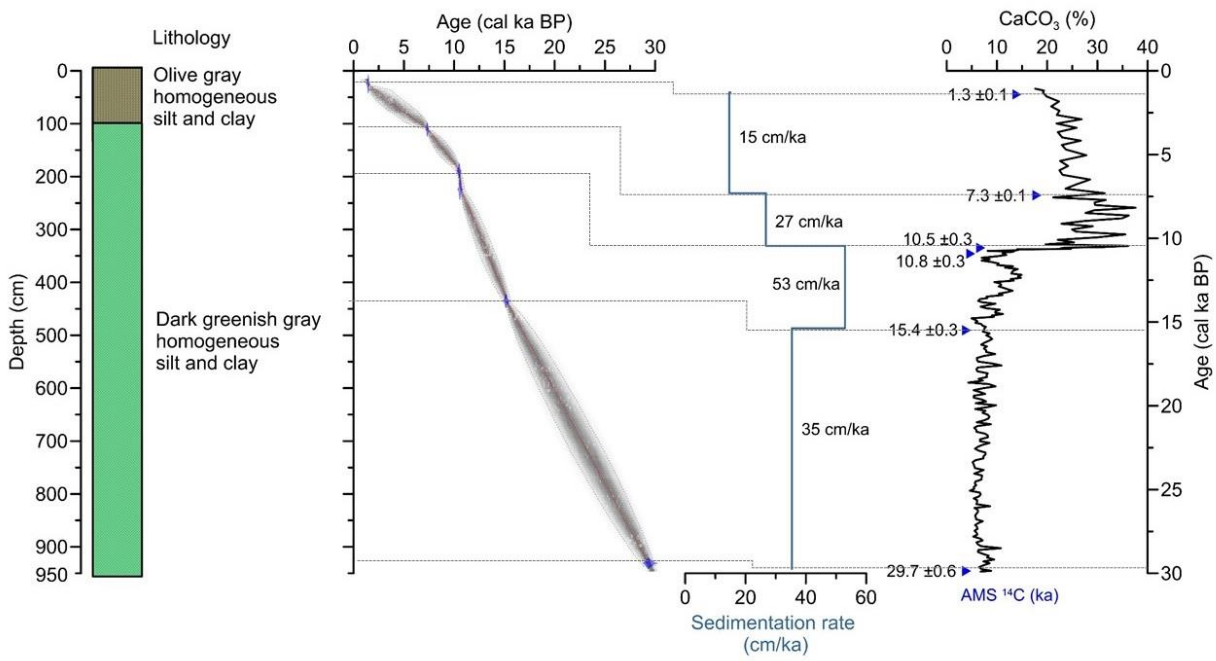

Figure 2. Lithology and age model of Core SO18383-3 showing lithology, foraminiferal AMS ^{14}C datings (blue triangle), sedimentation rate, and carbonate content. The age depth relationship was calculated with the Bayesian statistic by using the Bacon age-modelling (Blaauw and Christen, 2011) overlying the distributions of the individual dates (blue). Line curve shows the best model (red line: mean), area between blue lines indicate chronological uncertainties (the model's 95% probability interval).

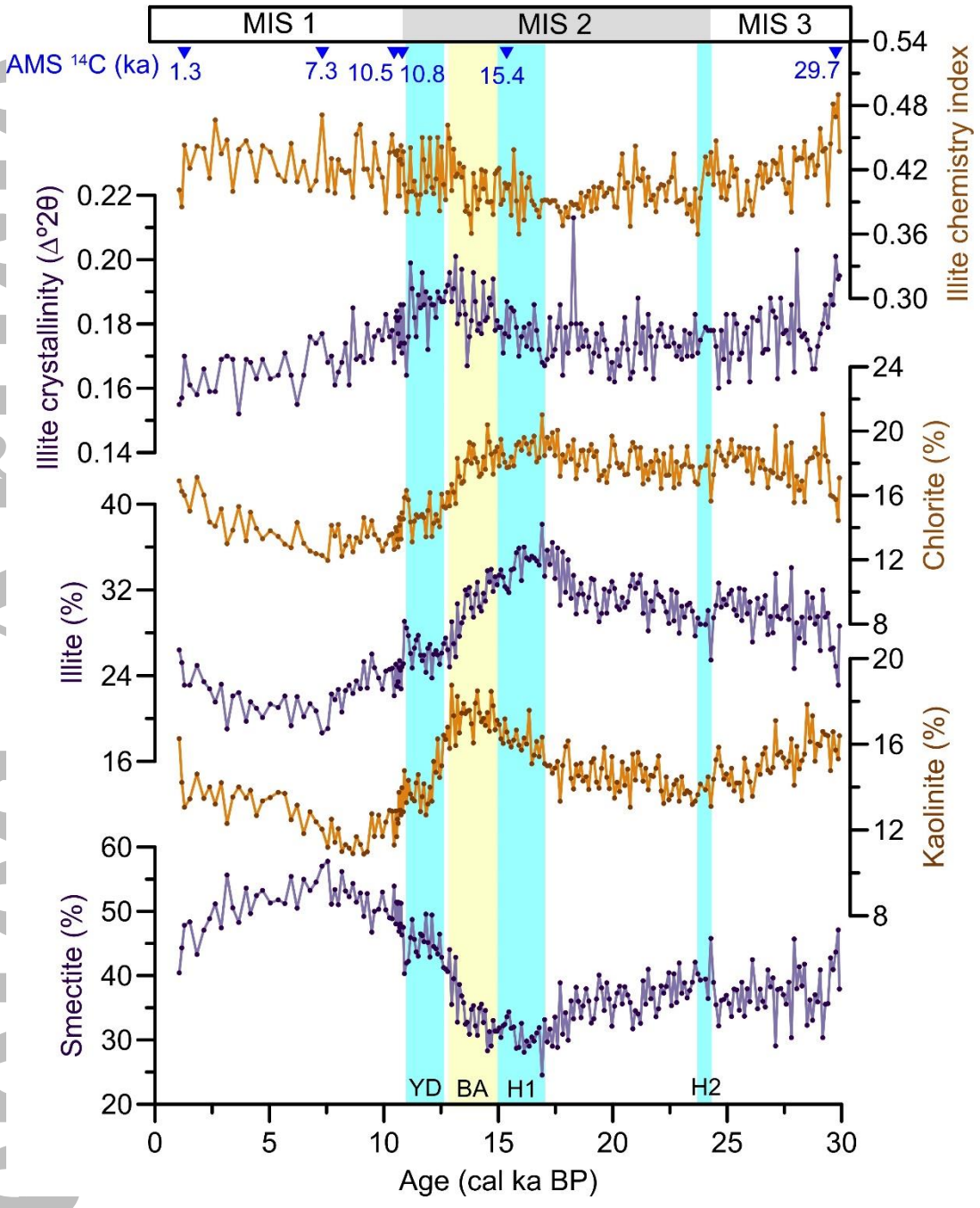

Figure 3. Temporal variations in clay mineral assemblage of Core SO18383-3. The foraminiferal AMS ^{14}C datings (blue triangle) is also displayed. The shaded bars indicate Heinrich Events (H1 and H2), Bølling–Allerød (BA), and the Younger Dryas (YD) (Wang et al., 2001).

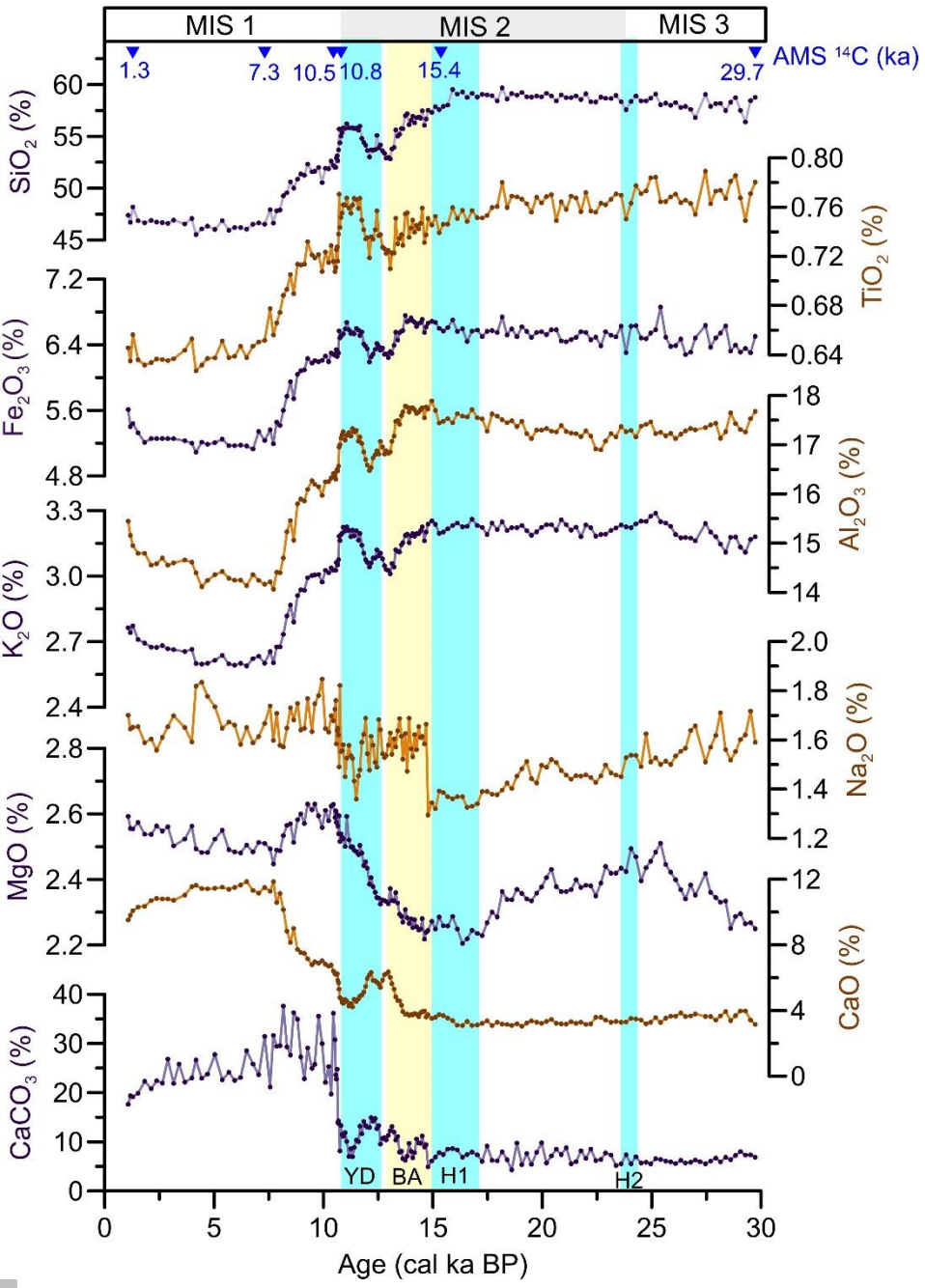

Figure 4. Temporal variations in major element contents of Core SO18383-3. The foraminiferal AMS ^{14}C datings (blue triangle) is also displayed. Carbonate content ($CaCO_3$%) shows a linear correlation to CaO (%). The shaded bars indicate abrupt climate events as in Figure 3.

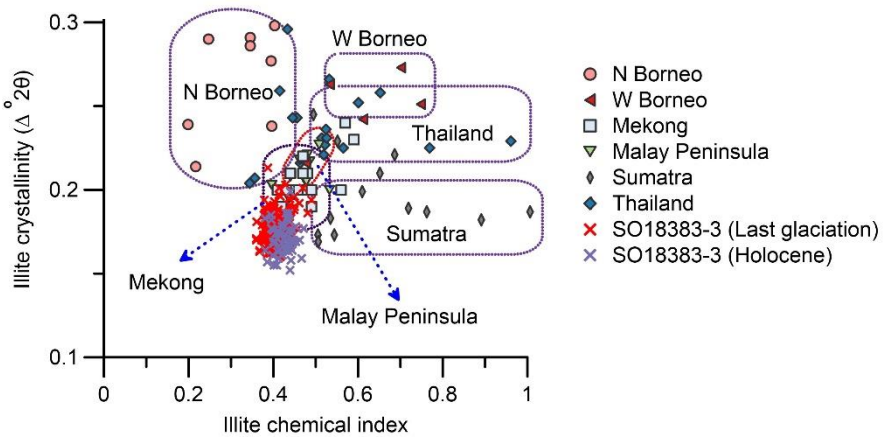

Figure 5. Ternary diagram of clay mineral assemblage of Core SO18383-3. Surrounding river samples for potential sediment sources are indicated for comparison, including the Mekong River and Thailand (Chao Phraya) river systems as well as river systems in Sumatra, Malay Peninsula, western (W) and northern (N) Borneo (Liu et al., 2007, 2012, 2016). Data of Core MD01-2393 from Liu et al. (2004). The arrow indicates the differential settling of smectite.

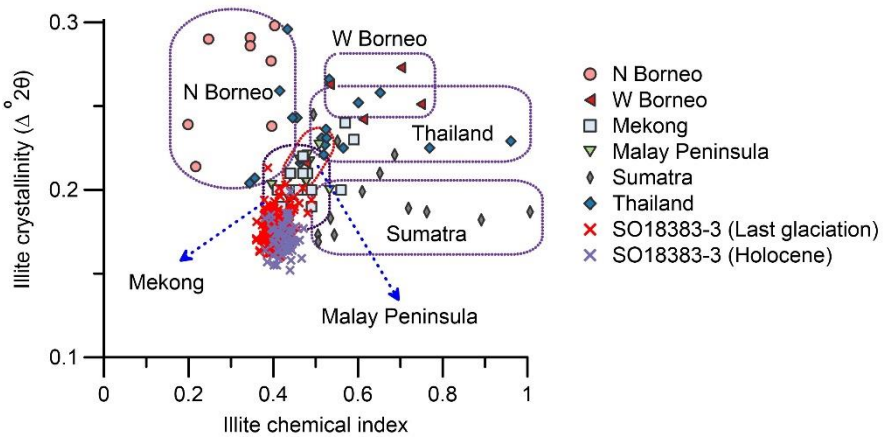

Figure 6. Illite provenance analysis of Core SO18383-3 based on the comparison of illite chemical index with illite crystallinity. Data of surrounding river samples as in Figure 5.

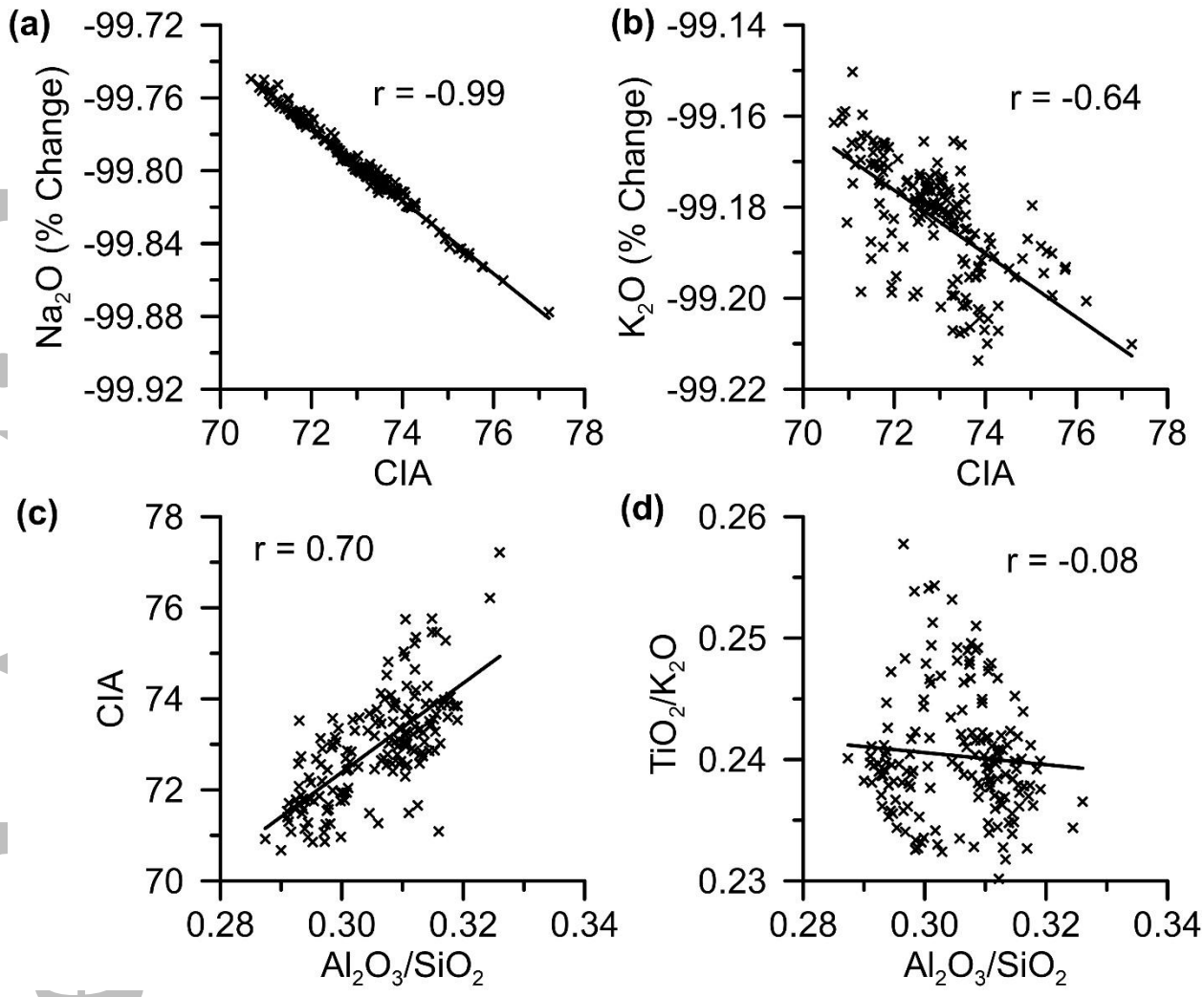

Figure 7. Correlation plots of CIA with percentage changes of (a) Na_2O and (b) K_2O; and of Al_2O_3/SiO_2 ratio with (c) CIA value and (d) TiO_2/K_2O ratio. Percentage change is calculated by normalization with Al_2O_3, comparing with the Na_2O/Al_2O_3 and K_2O/Al_2O_3 background values from average UCC (Taylor and Mclennan, 1985).

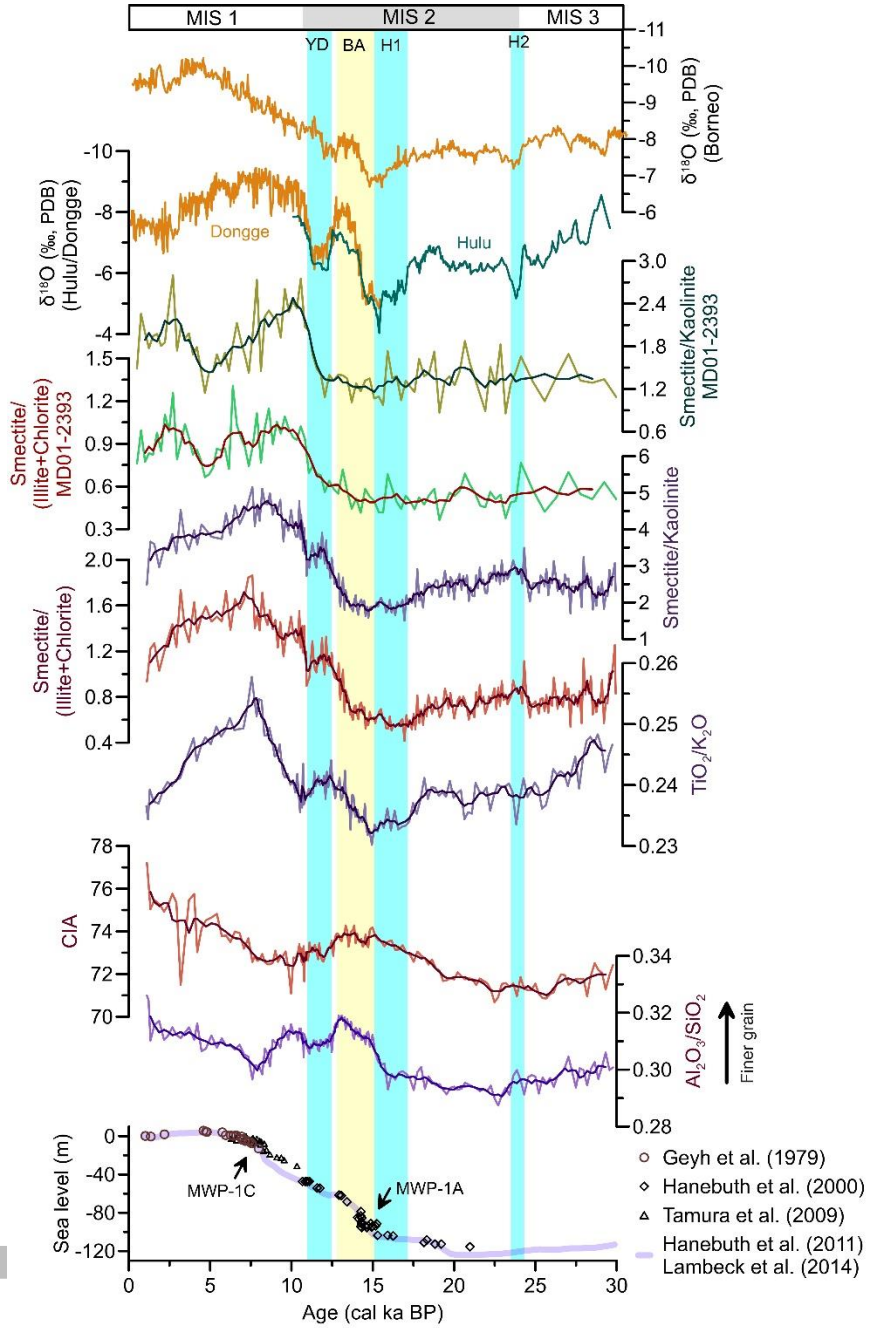

Figure 8. Temporal variations of chemical weathering proxies of Core SO18383-3 since the LGM and comparison with stalagmite $\delta^{18}O$ of Dongge, Hulu, and northern Borneo Caves from Wang et al. (2001), Dykoski et al. (2005), and Carolin et al. (2016). Clay mineral ratios of Core MD01-2393 are from Liu et al. (2004). Sea level data are from Geyh et al. (1979), Hanebuth et al. (2000, 2011), Tamura et al. (2009), and Lambeck et al. (2014). All parameters of Core SO18383-3 are smoothed with a five-point running average to obtain more general trends. The shaded bars indicate abrupt climate events as in Figure 3.